Available online at www.sciencedirect.com
SCIENCE DIRECT
Journal of Catalysis 235 (2005) 302–317
JOURNAL OF CATALYSIS
www.elsevier.com/locate/jcat

Solution syntheses of unsupported Co(Ni)–Mo–S hydrotreating catalysts

D. Genuit, P. Afanasiev *, M. Vrinat

Institut de Recherches sur la Catalyse, 2, Avenue Albert Einstein, 69626 Villeurbanne cedex, France

Received 30 April 2005; revised 25 August 2005; accepted 25 August 2005

Abstract

Highly dispersed Ni(Co)–Mo–S sulfides were prepared by simple room temperature solution reactions using nickel or cobalt salts and thiomolybdate precursors in the presence of nonionic surfactants. The products were characterized by X-ray powder diffraction, specific surface area measurements, and scanning and transmission electron microscopy. The evolution from amorphous pre-catalysts to highly dispersed sulfide catalysts during the activation step was studied by thermal analysis. Extended X-ray absorption fine structure measurements were carried out to elucidate the chemical environment of the transition metals in the precursors and the sulfided catalysts. The specific catalytic activities of the Ni(Co)–Mo–S systems in the hydrodesulfurization of thiophene and 4,6-DMDBT were up to six times higher than those of commercial alumina-supported systems.

Keywords: Sulfides; Cobalt; Molybdenum; Hydrotreating; EXAFS

1. Introduction

Because of the need to minimize the negative environmental effects of automotive and nontransportation exhaust emissions, the authorized sulfur level in motor fuels has been gradually decreasing during the recent years. Many different approaches have been proposed to eliminate sulfur-containing molecules from the petroleum feedstocks. Some of these proposals are based on novel processes, whereas others attempt to improve on the existing hydrotreatment (HDT) technology. Because of the much lower investment costs, the use of more active catalysts is the most attractive solution for petroleum refiners. Such a demand for more active HDT catalysts has triggered a significant increase in research activity on HDT catalysts [1–4]. These studies have shown in particular that one way to improve the MoS_2-based catalysts could be to increase the active phase loading or use bulk sulfides. The emergence of highly loaded sulfide catalysts [5,6] demonstrates that sulfide-based systems, even though known for many years, still have great potential for improvement.

Molybdenum disulfide (MoS_2) promoted with Ni or Co is the basis of commercial HDS catalysts [7–13]. It is commonly accepted that in the active structures of these catalysts, the promoter atoms are located at the edges of the MoS_2 sheets in the form of the so-called Ni(Co)–Mo–S structures. The catalytic activity is strongly dependent on the dispersion of the MoS_2 phase and the ratio of edge sites to basal plane area, as well as on the stacking of the MoS_2 slabs. Therefore, control of MoS_2 morphology is crucial to obtaining highly active HDS catalysts.

Various alternative methods for preparing dispersed MoS_2 have been developed recently, including thermal decomposition of thiosalts [14–16], hydrothermal and solvothermal processes [17–21], and solution reactions [22,23]. Thus prepared, bulk or highly loaded supported molybdenum sulfide can be further promoted by cobalt or nickel [24–26]. However, introduction of the promoter always represents a delicate procedure, and simple methods for one-step preparation of promoted sulfide dispersions still represent a challenge. The present work deals with such simple solution reactions.

2. Experimental

2.1. Preparation of the catalysts

Catalyst preparation was carried out in two stages. First, the pre-catalysts were prepared in the aqueous or mixed so-

* Corresponding author.
E-mail address: afanas@catalyse.cnrs.fr (P. Afanasiev).

0021-9517/$ – see front matter
doi:10.1016/j.jcat.2005.08.016

Table 1
Preparation conditions and properties of selected catalysts after sulfidation

Solid designation	Precursors and surfactant used	Chemical composition		S (m^2/g)	R(p)[a] (nm)	MoS_2 size, XRD (Å)	R(HDS), 573 K (10^{-8} mol/(g s))
		r[b]	C (wt%)				
Co-D–H_2O	TDM, $Co(NO_3)_2$, H_2O	0.19	Traces	52	2.1	37	30
Co-D–EG	TDM, $Co(NO_3)_2$, H_2O, EG (50%)[c]	0.24	0.9	31	1.8	31	62
Co-D–Ter	TDM, $Co(NO_3)_2$, H_2O, Tergitol (10%)	0.11	1.7	21	2.4	27	51
Co-D	TDM, $Co(NO_3)_2$, H_2O, EG (50%), Tergitol (10%)	0.28	4.3	132	2.4	24	213
Co-M	TMM, $Co(NO_3)_2$, H_2O, EG, Tergitol (10%)	0.48	2.8	114		29	151
Ni-D	TDM, $Ni(NO_3)_2$, H_2O, EG (50%), Tergitol (10%)	0.24	3.5	130	2.7	22	416
Ni-M	TMM, $Ni(NO_3)_2$, H_2O, EG (50%), Tergitol (10%)	0.51	2.6	122	10.5	38	111
CoA-D	TDM, $Co(acac)_2$, H_2O, EG (50%), Tergitol (10%)	0.23	2.6	134	4.1	25	275
NiA-D	TDM, Niacac, H_2O, EG (50%), Tergitol (10%)	0.24	3.5	132	7.5	22	461

[a] Mean pore size, nm.
[b] $r = Co/(Co + Mo)$ atomic ratio.
[c] EG—ethylene glycol, volume proportions are given.

lutions, and then they were sulfided by gaseous reactants. To prepare the pre-catalysts, high-purity starting materials were purchased from Sigma–Aldrich. Ammonium thiomonomolybdate $(NH_4)_2MoS_4$ (TMM) was obtained by adding 15 g of $(NH_4)_6Mo_7O_{24} \cdot 4H_2O$ to 200 ml of a 20 wt% aqueous solution of $(NH_4)_2S$ at ambient temperature. The precipitated red crystals were thoroughly washed with ethanol, dried, and stored under nitrogen. Ammonium thiodimolybdate $(NH_4)_2Mo_2S_{12}$ (TDM) was prepared as described previously [27]. Several substances of the same family of surfactants were tried as textural promoters. The length and the branching of the aliphatic tail, as well as the length of the polyethoxo fragment, were varied. Triton X114 [polyoxyethylene (8) isooctylphenyl ether], Triton X100 [polyoxyethylene (10) isooctylphenyl ether], Tergitol NPX [polyoxyethylene (9) nonylphenyl ether], and other grades of the same molecule Imbentin N 60 [polyoxyethylene (9) nonylphenyl ether] were tried as surfactants.

In a typical pre-catalyst preparation (Co-D specimen), 50 ml of aqueous solution containing 1 g (0.003 mol) of $Co(NO_3)_2 \cdot 6H_2O$ was added to a solution of 2 g (about 0.003 mol) of TDM in 100 ml distilled water, 100 ml of ethylene glycol (EG), and 30 ml nonionic surfactant Triton X114. The resulting dark precipitate was separated by centrifugation and dried overnight under vacuum at 353 K. To obtain the sulfide catalyst, the dried pre-catalyst was sulfided in flowing 15 vol% H_2S in H_2 at atmospheric pressure at 723 K for 4 h. The sulfiding gas flow was 3.6 l/h, and the heating rate was 5 K/min. Several synthesis parameters were varied, including the nature of the reactants and surfactant and the ratio of the transition metals in the solution. The solid designations are listed in Table 1.

Commercial supported catalysts containing 3 wt% Co(Ni) and 10 wt% Mo supported on gamma alumina were used as references. These were sulfided under the same conditions as the unsupported solids.

2.2. Characterization of the solids

The N_2 adsorption and desorption isotherms were measured on a Micromeritics ASAP 2010 instrument. Pore size distributions of the samples in the mesopore domain were calculated from the isotherms by the Barrett–Joyner–Hallenda (BJH) method. The BJH pore size distributions were calculated from the desorption branch of the isotherms. The X-ray diffraction (XRD) patterns were obtained on a Bruker diffractometer with Cu-K_α emission; the diffractograms were analyzed using the standard JCPDS files. MoS_2 particle size was determined using Scherrer's equation.

Chemical analyses were carried out using the atomic emission method. Scanning electron microscopy (SEM) images were obtained on a Hitachi S800 device at the CMEABG center of Lyon Claude Bernard University. Transmission electron microscopy (TEM) was performed with on a JEOL 2010 device with an accelerating voltage of 200 keV. Thermal analysis was carried out on a Setaram device under inert gas flow at a heating rate of 5 K/min. The gaseous products evolved on heating of the samples were studied using a mass spectrometer (Gas Trace A; Fison Instruments) equipped with a quadrupole analyzer (VG analyzer) working in a Faraday mode. A silica capillary tube heated at 180 °C continuously bled off a proportion of the gaseous reaction products.

The extended X-ray absorption fine structure (EXAFS) measurements were performed at the Laboratoire d'Utilisation du Rayonnement Electromagnétique (LURE, Orsay, France), on the XAS 13 spectrometer using a Ge (400) monochromator. The measurements were carried out in the transmission mode at the Co K edge (7709 eV), Ni K edge (8333 eV), and Mo K edge (20000 eV) at ambient temperature, with 2 eV steps, 2 s per point. The sample thickness was chosen to give an absorption edge step of about 1.0 near the edge region. Phase shifts and backscattering amplitudes were obtained from FEFF [28] calculations on model compounds. FEFF calculations for the pre-catalysts were done using the ICDS structures of the corresponding TMM and TDM precursors; and for the sulfided Co(Ni)MoS phases using the MoS_2 structure for the Mo edge and for the Co edge by replacing the Mo scatterer by cobalt in the MoS_2 structure. The EXAFS data were treated with the VIPER program [29]. Background extraction after the edge was carried out using Bayesian smoothing with a variable number of knots. The curve fitting was done alternatively in R and k spaces, and the fit was accepted only in the case of simultaneous convergence (absolute and imaginary parts for the R space). Coordination numbers (CN), interatomic distances (R), Debye–Waller parameters (σ^2), and energy shifts (ΔE_0) were used as fitting variables. Constraints were introduced relating the fitting parameters, to obtain the values lying in physically reasonable intervals. The quality of fit was evaluated using the values of variance and goodness. Comparisons between the models using different numbers of parameters were made based on the F-test. Second-shell Mo and Co backscatters were identified by the difference file technique with phase-corrected Fourier transforms [30].

2.3. Catalytic tests

Catalytic activity for thiophene hydrodesulfurization (HDS) was measured at atmospheric pressure in a fixed-bed flow microreactor. In the temperature range 573–613 K, the thiophene conversion was <30% under the conditions used (50 ml/min gas flow, 50–60 mg catalyst), and the plug-flow reactor model was used to calculate the rate constant

$$k = \frac{F}{mC} \ln \frac{1}{1-x},$$

where k is the pseudo-first-order rate constant ($m^3/(g\,s)$), F is thiophene molar flow (mol/s), m is catalyst mass (g), C is thiophene molar concentration (mol/m^3), and x is conversion determined after 15 h time on stream.

Catalytic tests for the HDS of 4,6-dimethyldibenzothiophene (4,6-DMDBT) were carried out in a three-phase continuous flow microreactor with dodecane as the solvent, working with a total mass liquid flow of 3.8 g/h, $P_{tot} = 3$ MPa, and H_2 flow = 26 cm^3/min, at three different temperatures (533, 553, and 573 K). The catalyst mass was approximately 30 mg. The 4,6-DMDBT content in dodecane was 300 ppm. The products were analyzed by gas chromatography.

The specific rate was calculated according to the following expression:

$$r = \frac{F}{m}(\mathrm{Conv_{DBT}}),$$

where r is the specific rate ($mol/(g\,s)$), F is the molar flow rate of the reactant (mol/s), $\mathrm{Conv_{DBT}}$ is the conversion of DMDBT, and m is the catalyst weight (in g). All rates were estimated at low conversion (<15%).

3. Results and discussion

3.1. Solution syntheses and properties of the products

3.1.1. The choice of synthesis route

The goal of this work was to find a simple and reproducible technique to allow the preparation of high-surface area unsupported promoted Co(Ni)–Mo sulfides. Several preparation approaches were tried and rejected, including modifying the homogeneous sulfide precipitation [31], decompositing impregnated thiomolybdate [32], and coagulating the MoS_x nanospheres prepared as described previously [33] with solutions of Co or Ni salts. All of these techniques produced catalysts with moderately good activity, but the properties of the obtained solids were difficult to reproduce, probably because in all of these cases, the efficiency of the promoter distribution over the molybdenum sulfide depended on the macroscopic parameters, such as solution stirring and drying conditions. To obtain homogeneous sulfide dispersions in a reproducible manner, we looked for a technique that binds Co and Mo together through a stoichiometric reaction that is as simple as possible and preferably occurs spontaneously at ambient conditions. The reaction of Co(II) or Ni(II) salts with thiomolybdates appeared to provide such a process if the conditions were properly adjusted, as described later in the paper. In these reactions, cationic species of VIII group metals interacted with thiomolybdate anions, leading to precipitation of solids, according to the following hypothetical reactions:

$$Co^{2+} + MoS_4{}^{2-} \Rightarrow CoMoS_4 \quad (1)$$

and

$$Co^{2+} + Mo_2S_{12}{}^{2-} \Rightarrow CoMo_2S_{12}. \quad (2)$$

The key step in obtaining highly dispersed catalysts using these reactions is choosing the solvent and the organic admixture used as a textural promoter.

The aqueous reaction of thiomolybdates with Co(II) or Ni(II) salt solutions led to the immediate formation of black precipitates, but their further sulfidation produced solids with quite low HDS activity. Moreover, although monothiomolybdate is sufficiently soluble, the dithiosalt is less soluble in water, so that the aqueous solutions used for the preparations must be inconveniently diluted (<1 wt%). Adding EG to the reaction mixture drastically increased the solubility of TDM and also improved the catalytic properties of the obtained solids. However, the resulting catalysts remained less active than the commercial alumina-supported reference systems. A real improve-

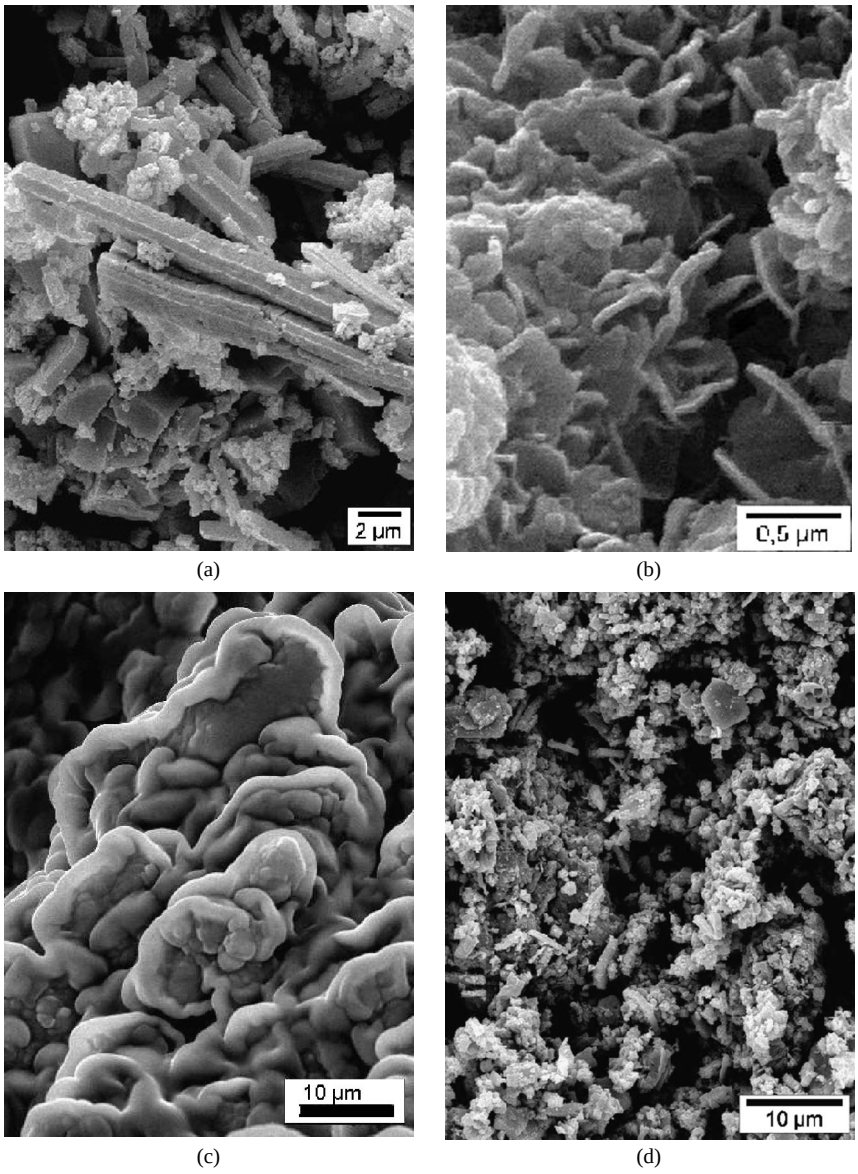

(a) (b) (c) (d)

Fig. 1. SEM images of the TDM precursor (a), the pre-catalyst obtained from pure aqueous solution (b), the Co-D pre-catalyst issued from the mixed solution with surfactant (c) and the solid (c) after sulfidation (d).

ment was achieved only after adding a textural promoter, a nonionic surfactant that is a member of the alkyl aryl-polyethylene glycol family. We conclude that a reaction mixture that provides good textural properties necessarily includes both EG and surfactant. Indeed, the same preparation carried out with addition of the Tergitol surfactant but without EG demonstrated low activity (Table 1). It can be speculated that EG acts as a solubilizing agent, whereas the surfactant presumably provides the organic species that remain in the precipitate and are transformed to carbonaceous matter on further sulfidation. Indeed, the carbon content in both the nonsulfided catalysts and the sulfidation products was higher for the surfactant-assisted preparations (Table 1). The stabilizing role of carbonaceous residuals for the morphology of unsupported sulfides was noted previously [22]. Moreover, Chianelli and Berhault [34] suggested that carbon is needed to create the active metal carbosulfide phases.

As shown in the SEM studies, the pre-catalysts obtained from the mixed solvent–surfactant system have a smooth "rose-like" morphology that was transformed by sulfidation to a fine dispersion (Fig. 1). This morphology is characteristic of our syntheses, appearing in virtually all of the solids obtained with participation of EG and a nonionic surfactant. All of the pre-catalysts are dense, glue-like bodies with no porosity.

3.1.2. Thermal analysis of the thiomolybdate salts and the pre-catalysts

The evolution of the surfactant-containing pre-catalysts during their activation in the H_2S/H_2 mixture occurred with high mass losses and significant changes in the volume of solids. Simultaneously, intense gas production occurred, mostly in the temperature range 473–623 K. Although the TDM precursor already contained molybdenum in the sulfided state, applying the reducing gas flow appeared to be important for efficiently

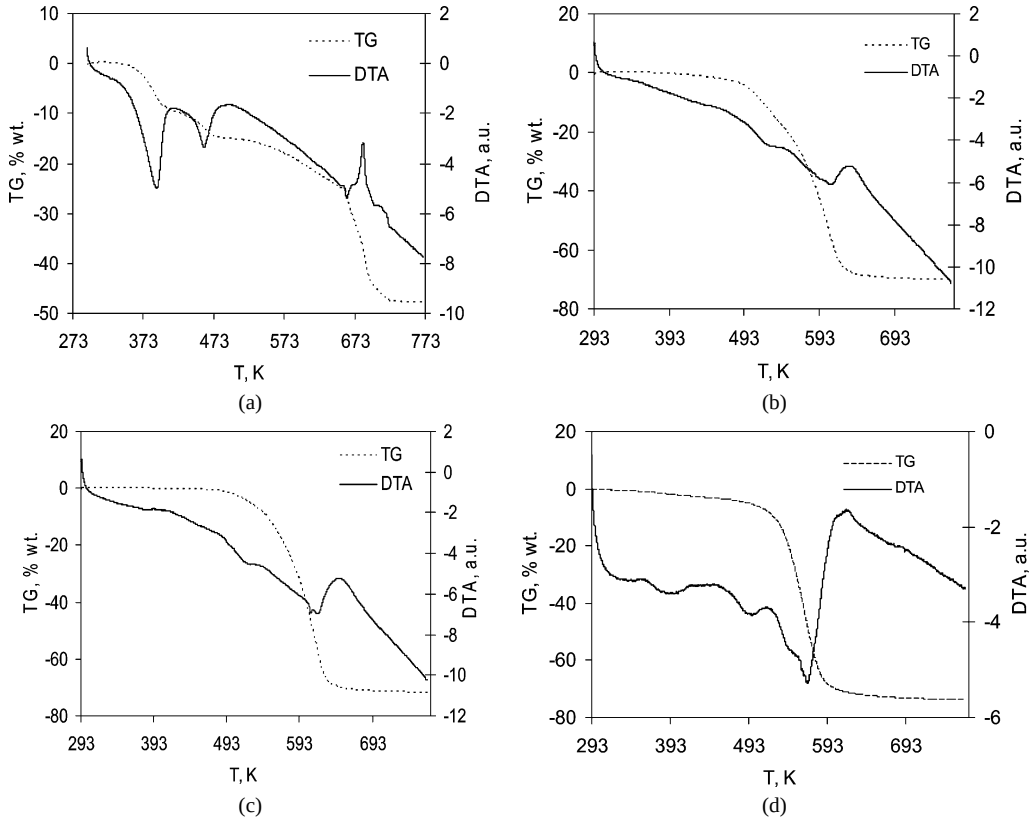

Fig. 2. Thermal analysis curves for the TDM parent salt (a), the Co-D pre-catalyst (b), the Ni-D pre-catalyst (c), and the Co-M pre-catalyst (d).

evacuating carbon-containing decomposition products and obtaining highly active catalysts.

Decomposition of both Ni-D and Co-D pre-catalysts and the initial TDM compound was studied under a flowing 5% H_2/N_2 mixture by TG-DTA coupled with mass spectrometry of the evolved gases, with the goal of understanding the nature of the decomposition processes. The results of these measurements are presented in Fig. 2. The thermal decomposition of hydrated $(NH_4)_2Mo_2S_{12}$ has been studied previously [35–37], and the reaction sequence (3) and (4) has been proposed to describe this process:

$$(NH_4)_2Mo_2S_{12} \cdot 2H_2O \rightarrow \text{“}Mo_2S_{11}\text{”} + 2NH_3 + H_2S + 2H_2O \quad (3)$$

and

$$\text{“}Mo_2S_{11}\text{”} \rightarrow 2MoS_2 + (7/8)S_8. \quad (4)$$

Alternatively, when the decomposition is carried out under hydrogen, the last reaction might be partially or totally replaced with reaction (5), which has the same mass loss as reaction (4),

$$\text{“}Mo_2S_{11}\text{”} + 7H_2 \rightarrow 2MoS_2 + 7H_2S. \quad (5)$$

Our TG-DTA analysis and mass spectrometry results corroborate these equations. The TDM salt decomposed to give amorphous molybdenum sulfide (“Mo_2S_{11}”) as an intermediate product. The amorphous nature of the Mo_2S_{11} solid follows from the X-ray powder pattern (not shown), which exhibited just broad humps with no sharp reflections. After the first two endothermic peaks (Fig. 2a), the mass loss was 15.3%, whereas the theoretical value for the reaction (3) was 15.4%. From the TG curve, it is clear that this event consisted of two steps, and the mass spectra showed that NH_3 ($m/z = 17$), H_2O ($m/z = 18$), and H_2S ($m/z = 34$) were emitted. After this event, the mass change starting from about 500 K was smooth and accompanied only by emission of small amounts of hydrogen sulfide. Then a sharp and strongly exothermal event occurred in the range 660–710 K, accompanied by the emission of sulfur ($m/z = 32$) and H_2S ($m/z = 34$). The total experimental mass loss of 48.9% up to 773 K was slightly lower than the value of 50.6% expected for the combination of reactions (3)–(5). Thermal and reductive decomposition of MTM and TDM was studied in detail by Brito et al. [35], who, in agreement with our results, observed a strong exothermal event at about 673 K regardless of gas flow.

Investigation of the pre-catalysts Co-D and Ni-D under the same conditions showed that, in contrast to the parent TDM, their decomposition started at only about 473 K (Figs. 2b and 2c). The absence of any important mass loss between 273 and 473 K suggests that the hydrating water and the ammonium ions from the parent salts were no longer present in the pre-catalysts. On further heating, the sample mass decreased smoothly from 473 to 573 K, then accelerated somewhat above 573 K. At 623 K, the decomposition was nearly accomplished. (That of the parent TDM salt was not finished until 723 K.) Simultaneous with the mass loss was the emission of several gases, including H_2O, CO, and H_2S and many organics, among which the dominating species detected by mass spectrometry were CH_2O ($m/z = 30$) and CH_4 ($m/z = 18$; to distinguish its sig-

nal from that of water, the signals at $m/z = 14$ and 15 were analyzed). The mass loss was monotonous with no noticeable steps. Because the pre-catalysts are complex composites with no well-defined chemical formulas, chemical equations cannot be written down to calculate the mass losses. However, for all of the pre-catalysts the mass losses were about 70 wt%, which corresponds to removal of all extra matter, leaving only metals in the sulfided state in the solids. During the decomposition of the TDM-derived pre-catalysts, two smooth endothermic events were observed, one at about 533 K and another at 603 K. The Co-M specimen obtained from the monothiomolybdate behaved similar to the Co-D and Ni-D solids (Fig. 2d). Compared with the decomposition of the parent MTM, which exhibits a sharp exothermic peak at 673 K [35], the decomposition of Co-M was smooth and shifted to lower temperatures by at least 100 K. The DTA curve in this case was more complex and included several endothermic events.

Two important conclusions follow from the thermal analysis results that may provide insight into the relation between pre-catalyst composition and the high activity of the final catalysts. First, the reductive transformation of the pre-catalysts to molybdenum sulfide occurred at considerably lower temperature than that of the parent thiomolybdate salts, which is obviously favorable for obtaining dispersed sulfides. Second, no exothermic events were observed during the decomposition of the pre-catalysts. In all likelihood, the large amount of organics that are eliminated with endothermic effects prevents rapid crystallization of MoS_2, thus preserving it in a highly dispersed state.

XRD showed that the pre-catalysts are amorphous, whereas further sulfidation yielded dispersed MoS_2 (Fig. 3) with no cobalt-containing crystalline phases. Rietveld refinement of the XRD patterns gave the degree of stacking for the (002) broad peak, in the same sequence as that of the specific surface area

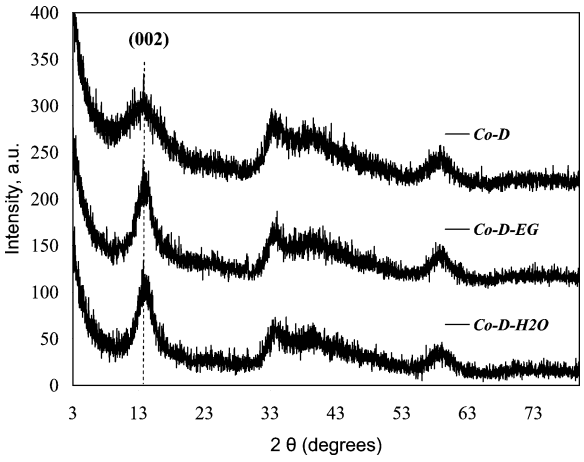

Fig. 3. Powder X-ray diffraction patterns after sulfidation.

values. TEM of the sulfided catalysts showed the presence of short MoS_2 fringes as a unique feature (Fig. 4). An EDS study revealed that the solids were highly homogeneous, with almost the same Co/Mo atomic ratio (fluctuating between 0.45 and 0.6) within the limits of the EDS spot resolution, which in our case was 15 nm. Moreover, the length of the slabs and their stacking (estimated as 3.3 nm and 3 slabs per crystallite, respectively) were much lower than those of the MoS_2 material issued from the TDM decomposition (11 nm and 7 slabs), as shown in Fig. 4c.

Summarizing the foregoing results, we can state that a simple room temperature synthesis has been developed that enables us to obtain pre-catalysts that can be transformed by further sulfidation to highly active HDS catalysts. The preparation includes reaction of TDM with cobalt nitrate in a mixed solvent in the presence of a nonionic surfactant. Although no systematic study was carried out for screening of different solvents

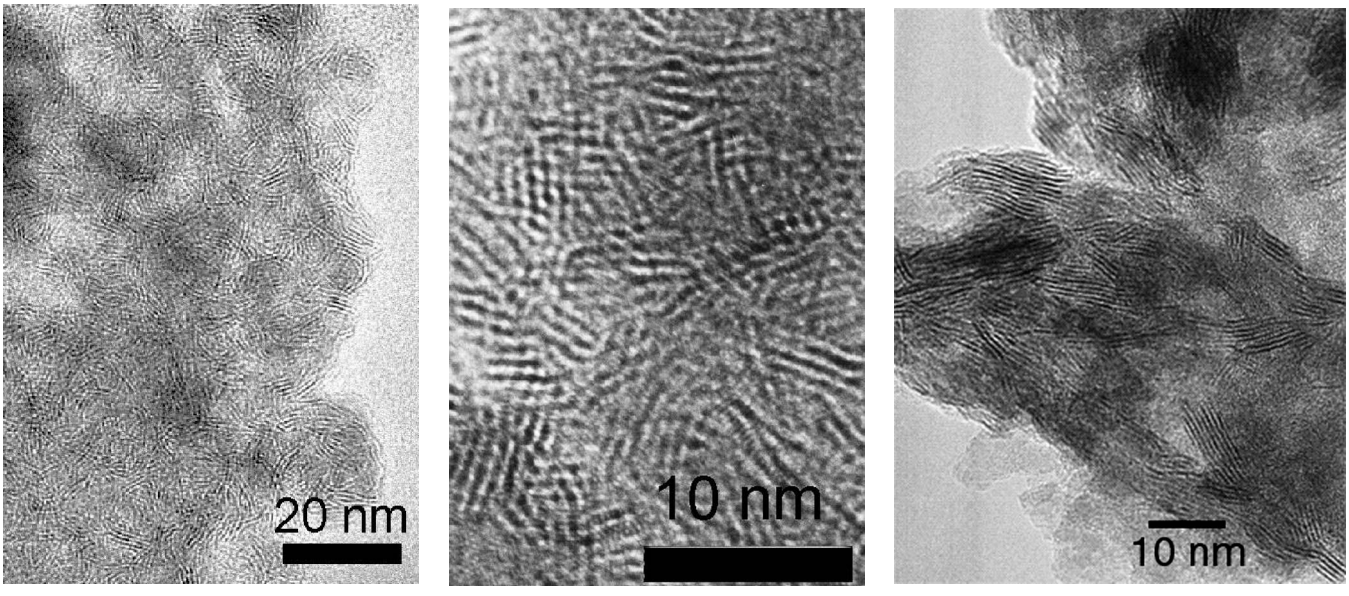

(a) (b) (c)

Fig. 4. Transmission electron microscopy images of the sulfided Co-D solid at the magnifications 400 000 (a) and 800 000 (b); the product of TDM decomposition observed at the magnification 400 000 (c).

and textural promoters, similar reactions in formamide and dimethylformamide were studied previously (thiomolybdates are easily soluble in these highly polar solvents), but the resulting catalysts had moderate surface areas and HDS activity. Tetraalkylammonium-based surfactants were also studied, similar to the systems described previously [22], but despite good textural properties, their HDS activities were again low, probably due to the poisonous nitrogen-containing residuals issued from the decomposition of alkylammonium moieties. In addition, polyvinylpyrrolidone was tried as a textural promoter in similar conditions, but without success. Of course, this does not mean that the route described in this work provides the only and best solution to the problem.

3.2. Optimization of the textural and catalytic properties

After establishing the general approach to the synthesis of Ni(Co)–Mo–S solids, we proceeded to a more detailed study of various synthesis parameters to better understand and optimize this technique. The HDS of thiophene was chosen as a screening reaction; the specific surface areas and/or nitrogen adsorption–desorption loops of the solids were compared simultaneously. There often is close similarity in the behavior of cobalt and nickel in reactions with thiomolybdates, but there also are strong differences, particularly in the catalytic properties of the solids obtained. In what follows, sometimes only cobalt is discussed, with the assumption that the same holds for nickel as well. In other instances, the differences between the two metals are emphasized.

3.2.1. Influence of the nature of the molybdenum source

The influence of the molybdenum source was quite straightforward in terms of the composition of the precipitates. If reactions (1) and (2) occurred, then the amount of cobalt fixed in the precipitates should be strongly affected by the nature of the thioanion used. Indeed, chemical analysis confirmed that the amount of cobalt was approximately two times higher in the TMM-derived solids than in the TDM-derived solids (Table 1). After sulfidation, the solids obtained from the TMM precursor always contained considerable amounts of cobalt sulfide, Co_9S_8. An excessive amount of cobalt led to segregation of the bulk Co_9S_8 phase, whereas the surface areas and porosities of the TMM-derived solids prepared using Co and Ni nitrates were at least as good as those of the TDM counterparts. The specific surface areas were slightly lower, but pore sizes and volumes were considerably greater (Fig. 5), which is generally considered an advantage for hydrotreating catalysts. In contrast to TDM, the TMM-derived specimens had very large pore size distributions, with mean pore sizes close to 10 nm. The products of the TMM reactions with Co and Ni acetylacetonates had very low surface areas (10–20 m^2/g) and are not discussed in this paper.

Earlier, bisthiometalato complexes of the type $[M'(MS_4)_2]^{n-}$ ($n = 2$ or 3, $M' =$ Co or Ni, and M = Mo or W) were used as precursors for the preparation of hydrotreating catalysts, but the catalytic activities as well as specific surface areas were moderate [38]. In contrast, decomposition of TDM reportedly

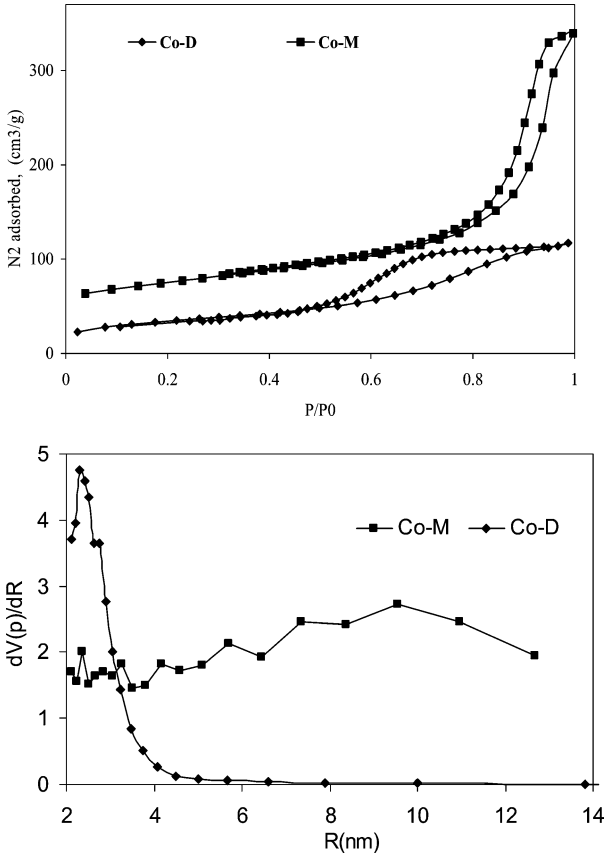

Fig. 5. Nitrogen adsorption–desorption isotherms for the sulfided solids Co-M and Co-D (a) and the BJH pores distribution (b). The isotherm of CoM is shifted up by 50 scale units for better presentation.

yielded mesoporous solids with a somewhat higher surface area than that of the product of TMM decomposition under the same conditions (50 m^2/g) [36]. We did not observe any advantage of the TDM over the TMM precursor in terms of textural properties; however, because TDM systematically led to higher HDS activity than TMM, our study was focused mostly on the TDM-derived specimens.

We also studied the trimolybdate $Mo_3S_{13}^{2-}$ ammonium salt, but its poor solubility in water and alcohols prevented us from using it as a precursor. Thermal decomposition of this salt in the H_2S/H_2 mixture resulted in solids with surface areas of 1–5 m^2/g. Earlier, the $Mo_3S_{12}^{2-}$ anion in combination with nickel was applied to obtain highly active alumina-supported HDS catalysts using the impregnation technique with dimethylformamide solutions [39]. Among the great variety of existing thiomolybdates, other anions, such as $Mo_2S_9^{2-}$ or $Mo_2S_8^{2-}$, might provide optimal stoichiometry of the precipitates [40–42]. However, the existing preparation methods for these thioanions are far more complex than those for TMM, and TDM.

3.2.2. Influence of the organic surfactant admixture

The variation in HDS activity as a function of the surfactant molecule used was minor (Fig. 6). Similar chemical compositions and very similar morphologies of the pre-catalysts were obtained using different grades of Tergitol, Imbentin, or Triton.

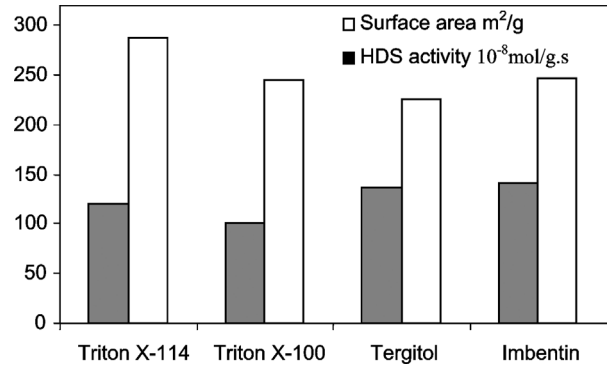

Fig. 6. Thiophene HDS rate constants measured at 573 K and surface areas of the pre-catalysts prepared using different surfactants grades.

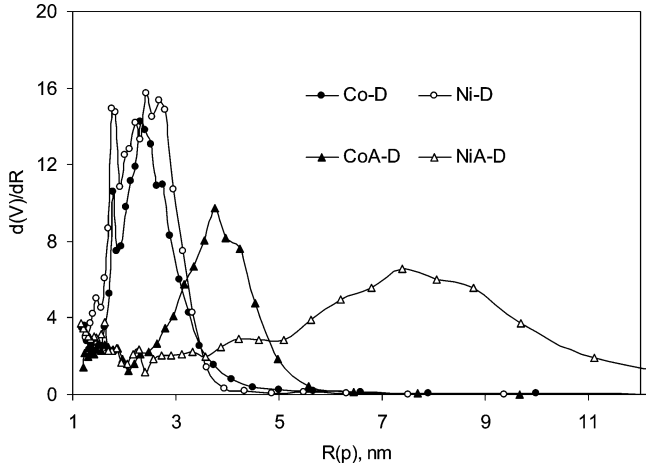

Fig. 7. Pore size distribution in the catalysts sulfided at 673 K.

Such a weak dependence indicates that no particular composition, but rather a wide variety of chemically similar surfactant molecules, is suitable for our preparations. More generally, as follows from our previous results [21,22] and literature data [43–45], numerous organic chemicals can be used to improve the HDS activity of sulfides with relatively good results. Indeed, various oxygenated compounds, including triethylene glycol, EG, and triethylene dimethyl glycol, can be applied to improve catalytic activity [44,45]. We suppose that carbonaceous species formed through the decomposition of these organic counterparts during the sulfiding treatment of the catalyst precursors disperse well over the sulfide particles, preventing MoS_2 slabs from sintering. The efficiency of such an approach was illustrated earlier by the fact that pure MoS_2 cannot be prepared with BET surface areas exceeding 50–60 m^2/g, whereas the materials containing some carbon exhibit stable surface areas attaining 300–400 m^2/g and have considerably higher catalytic activity than pure MoS_2 [21].

3.2.3. *Influence of the nature of the Co and Ni precursors*

Earlier, we observed that impregnation of dispersed unsupported MoS_2 or of supported, pre-sulfided MoS_2/Al_2O_3 catalysts with aqueous $Co(NO_3)_2 \cdot 6H_2O$ led to a poor promoting effect [25,26]. The negative influence of cobalt nitrate was explained by the oxidative destruction of MoS_2 by nitrate anions, an effect that was particularly pronounced in aqueous solution. In an attempt to avoid this phenomenon, we used cobalt acetylacetonate, $Co(acac)_2$, as a promoter and obtained a much better promotion effect [25]. It was therefore of interest to verify for the preparations under study whether the use of acetylacetonate has a beneficial effect on catalytic performance. Thus we replaced cobalt or nickel nitrate by the equivalent amount of the methanol solution of the corresponding acetylacetonate, keeping all other catalyst treatment procedures the same. The results of the HDS tests (Table 1) showed a slight advantage for the acac-derived solids over their nitrate-derived counterparts. The specific surface areas of the acac-derived solids were equal to those of their nitrate counterparts, whereas their porosities were much better developed (Fig. 7). However, the difference between the nitrate and acac precursors was much lower than that observed earlier [25]. This might be explained by the differing mechanisms of catalyst genesis. In the previously reported preparations, the nitrate solution was brought into direct contact with the MoS_2 surface and was thus able to oxidize it. In this work, the nitrate ion served merely as a charge-compensating species in the Co precursor and was present only in trace amounts in the pre-catalyst. Therefore, the differences between nitrate and acetylacetonate probably exist only on the level of nucleation and growth kinetics during the precipitation step. We suppose that other soluble salts of cobalt or nickel, such as sulfate, chloride, or acetate, can be used for this type of preparations with the same success.

The slightly acidic pH of the cobalt nitrate solution was suspected to be the reason for the nonstoichiometry of the Co–Mo precipitate (see below). To improve the reaction conditions and ensure strictly stoichiometric precipitation, we tried to carry out the precipitation under basic conditions, using soluble ammoniac complexes, obtained by adding aqueous ammonia to the nitrate solution, up to pH 12. Although the ammoniac cobalt complex reacts easily with TDM, the composition of the precipitate (atomic ratio of Co/Mo = 1.2) was not what we expected. The corresponding catalysts had a low activity and exhibited the presence of the Co_9S_8 phase after sulfidation. Apparently, reactions other than (1) and (2) also may occur under basic conditions.

3.2.4. *The influence of the Co/Mo atomic ratio in the reaction mixtures*

If the stoichiometric reactions (1) and (2) were the only processes occurring in solution, then there should be no dependence between the composition of the pre-catalyst composition and that of the reaction mixtures. In practice, however, it is well known that the composition of dispersed precipitates can be influenced by various phenomena, such as adsorption and occlusion. Furthermore, secondary reactions may be more or less important as functions of the reaction conditions. Therefore, the catalysts were prepared in solution with varying (Ni)Co/Mo ratios. The chemical compositions of the precipitates as a function of the (Ni)Co/Mo ratio in the solution are shown in Fig. 8. The amounts of nickel (cobalt) varied slightly, and were close to those expected from (1) and (2). This variation may be due to the slightly acidic pH of the nitrates, which could provoke par-

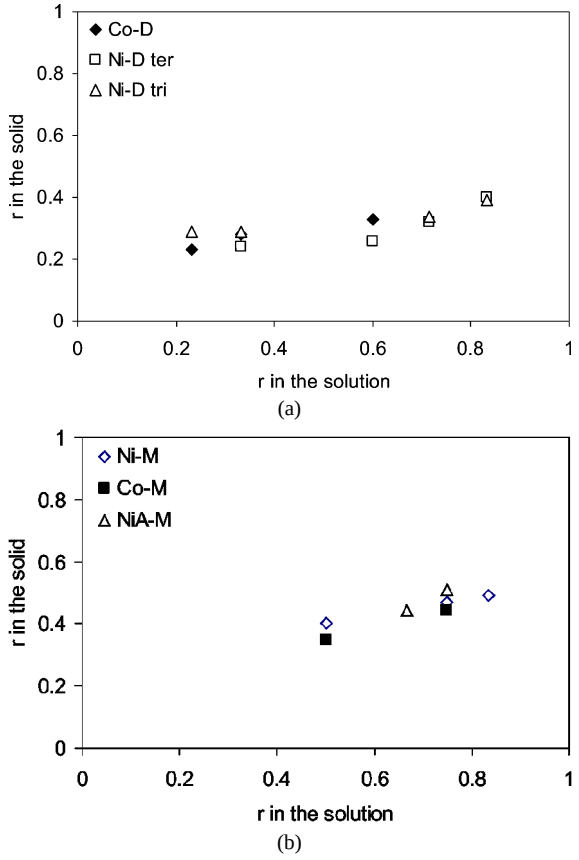

Fig. 8. Values of $r = \mathrm{Co}/(\mathrm{Co}+\mathrm{Mo})$ and $\mathrm{Ni}/(\mathrm{Ni}+\mathrm{Mo})$ atomic ratios in the solids as a function of the same parameter in the reaction mixture solution.

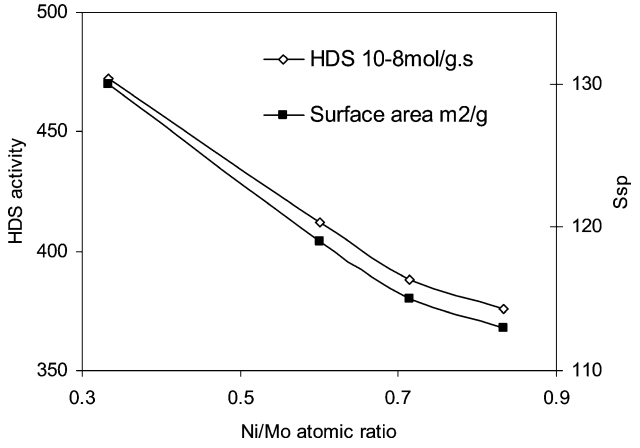

Fig. 9. Specific surface area and thiophene HDS rate constant at 573 K for Ni-D solids as a function of the initial Ni/Mo ratio in the reaction mixture solution.

tial precipitation of the amorphous binary sulfides MoS_3 and MoS_5 [33]. In agreement with the hypothesis on stoichiometric reactions, the (Ni)Co/Mo atomic ratio in the precipitates changed weakly on varying the (Ni)Co/Mo ratio in the solution. In contrast, the specific surface areas and HDS activities were significantly affected by the (Ni)Co/Mo ratio in the solution (Fig. 9). With high nickel or cobalt content, both the specific surface areas of the sulfided solids and their HDS activities decreased, even if no bulk sulfides were observed in the sulfided solids. Because the chemical and phase compositions of the precatalysts were not strongly affected, the origin of this effect is likely related to the influence of the concentration of the metal species on the kinetics of nucleation and growth of precipitate particles. A detailed study of such kinetics is beyond the scope of this work.

3.3. 4-6 DMDBT hydrodesulfurization activity

The ultimate goal is to synthesize catalysts for deep HDS that can remove the most refractory sulfur-containing molecules, such as alkyldibenzothiophenes, from the feeds. According to the literature [46–48], the transformation of 4,6-DMDBT occurs through two main parallel routes: the direct HDS pathway (DDS), which gives biphenyl (BP), and the hydrogenation route (HYD), consisting of a preliminary hydrogenation of one aromatic ring, yielding tetrahydro- and hexahydrodibenzothiophene or analogues (HN). These intermediates can be further desulfurized to cyclohexylbenzene (CHB). Other mechanisms exist, including isomerization, demethylation, and C–C bond scission in the DMDBT molecule before the HDS step. These mechanisms are less important for the conventional sulfide catalysts.

The results of catalytic tests given in Table 2 show that our catalysts had very high HDS activity, up to six times greater than those of commercial NiMo and CoMo alumina-supported systems per gram of catalyst. Moreover, our best unsupported catalysts were more active than the commercial references even per molybdenum atom (53 and 40 $\times$ 10^{-8} mol/(at s) at 573 K for Co-D and $CoMo/Al_2O_3$, respectively).

To test catalyst stability, we performed deactivation tests for at least 50 h and compared our catalysts with commercial references. During the first 50 h, deactivation was lower for the unsupported catalysts than for the NiMo reference.

The screening of HDS activity with the thiophene test provided only a qualitative estimate of the catalytic performance in 4,6-DMDBT desulfurization. There was no direct correlation between thiophene and 4,6-DMDBT HDS (Fig. 10), because the catalytic transformations of 4,6-DMDBT are obviously more complex than those of thiophene. In terms of total conversion, the same order of activity as in thiophene HDS was preserved, with nickel-containing systems slightly more active than their cobalt counterparts (Table 2). However, when cal-

Table 2
4,6-DMDBT conversion rates of unsupported catalysts and commercial references

Catalyst	Total 4,6-DMDBT conversion, 10^{-8} mol/(g s)	4,6-DMDBT HDS products, 10^{-8} mol/(g s)
	533–553–573 K	533–553–573 K
Co-D	4.8–10.5–23.4	3.9–9.6–22.1
CoA-D	3.7–7.1–15.5	3.2–5.5–13
Ni-D	3.9–8.8–23.1	1.5–4.9–19.4
NiA-D	5.3–12.5–24.8	1.5–4.0–15.2
Ni-M	2.5–4.5–7.1	1.6–2.7–4.3
Co-M	2.2–4.3–9.5	1.2–3.2–8.7
[a] $CoMo/Al_2O_3$	1.0–2.0–4.3	0.9–1.8–3.6
[a] $NiMo/Al_2O_3$	1.8–3.2–5.1	1.3–2.5–4.9

[a] Commercial reference.

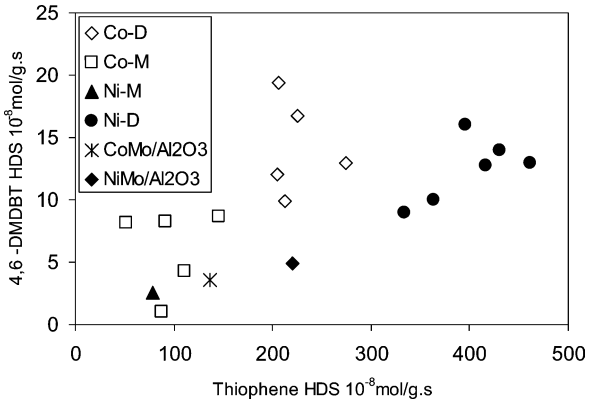

Fig. 10. Thiophene HDS rate vs. 4,6-DMDBT HDS rate at 573 K for the catalysts studied in this work.

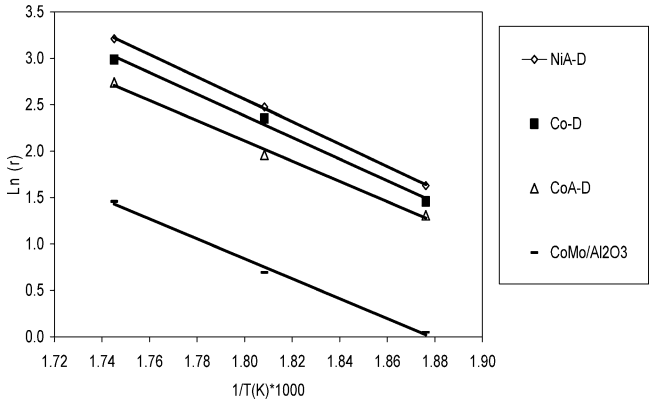

Fig. 12. Arrhenius plots of the 4,6-DMDBT HDS reaction rate for the unsupported catalysts and alumina-supported reference.

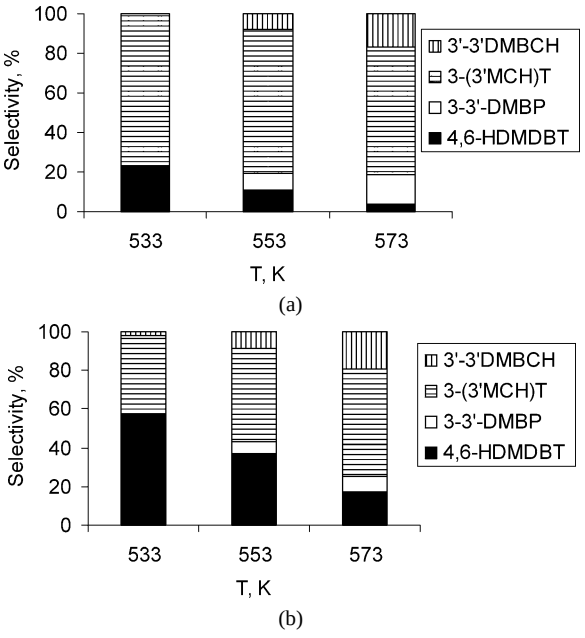

Fig. 11. DBT conversion selectivity for the Co-D (a) and Ni-D (b) catalysts as a function of the reaction temperature.

culated for HDS only, the cobalt and nickel-containing systems were virtually equal. The selectivity at the same conversion was much more in favor of direct HDS for the Co–Mo–S systems, whereas nickel-promoted catalysts were better in hydrogenation (Fig. 11), in agreement with previous studies [49–51].

The activation energies for the Co–Mo–S solids measured in the range 533–573 K were similar to those of the Co–Mo–S/Al_2O_3 reference (Fig. 12). This suggests that the active centers of the Co–Mo–S phase in the supported reference catalyst and our unsupported sulfides are similar. However, the unequal advantage of our systems over the reference catalyst in the reactions of thiophene (about two times) and 4,6-DMDBT (up to six times) remains unexplained. Differences in the acidity of the solids can be eliminated, because the selectivities of the supported and unsupported systems of the same chemical nature were similar. Moreover, at the pressure and temperature conditions of the 4,6-DMDBT HDS test, the solids were inactive in the isomerization of *o*-xylene. Therefore, the methyl group migration pathway should be of minor importance.

A possible explanation for the unequal thiophene and 4,6-DMDBT activity sequences might be the unequal distribution of CoMoS (I) and CoMoS (II) phases in the supported and unsupported catalysts [52,53]. Obviously, the unsupported catalysts contain more of the CoMoS (II) phase. A more highly stacked CoMoS (II) phase should be advantageous for the reaction of the large 4,6-DMDBT molecule, whereas the small thiophene molecule can easily be transformed on both type I and type II CoMoS phases [54]. Further elucidation of this question is needed, however.

3.4. EXAFS study of the pre-catalysts and the sulfided solids

Reactions (1) and (2) of pre-catalyst precipitation would remain hypothetic and the foregoing discussion purely speculative without a proper structural study of the pre-catalysts and sulfided solids. While the sulfided solids contained a dispersed MoS_2 phase, the pre-catalysts were very ill-defined and difficult to characterize. Indeed, all of the pre-catalysts were completely XRD amorphous and exhibited continuous total absorption on UV–vis diffuse reflection spectra. The broad XRD maxima were treated using the RAD program of Petkov to extract the radial distribution function (RDF) [55]. However, the resulting RDF (not shown) was almost featureless and dominated by a broad peak at ca. 2.4 Å, suggesting the presence of Mo–S bonds, a conclusion that contributes little to a better understanding of these systems. Raman spectra of the pre-catalysts were of poor quality as well. Broad peaks were observed at 320, 430, and 525 cm^{-1}, characteristic of the Mo–S and S–S bonds in the amorphous sulfides [56]. Again, this result was expected, and adds nothing to our knowledge of these solids. Moreover, a strong overlap in the vibration frequencies of Co_9S_8 and MoS_2 sulfides prevented us from distinguishing the lines of the corresponding species.

EXAFS is the most appropriate technique for elucidating the structure of amorphous or poorly crystalline solids. Several solids were studied by EXAFS before and after ex situ sulfidation to clarify the chemical identity of the pre-catalysts and the catalysts. For this study, accurate determination of the coordina-

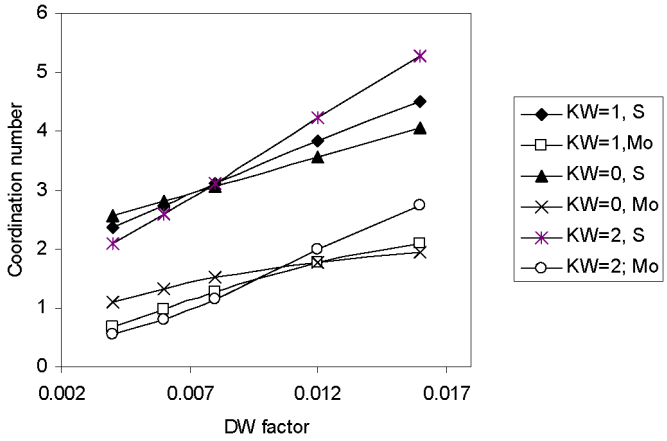

Fig. 13. Decorrelation of the Debye–Waller factor and CN parameters for Co K-edge sulfur shell in the CoD pre-catalyst. Curves correspond to the CN values obtained in the fit for different values of k weighting (KW).

tion numbers was particularly important, because the nature of the molybdenum neighbors (sulfur) obviously does not change from the thiomolybdate precursor to the pre-catalyst and further to the sulfided solid. Therefore, structural changes may be observed only on the level of the number of coordinating sulfur atoms and modifications of the distances. Extraction of the background is important to finding the true values, because it influences the intensity of $\chi(k)$ and then that of the FT modulus. Because there is no physically rigorous automatic algorithm of background extraction, we varied the regularizer α and the number of knots (KN) in the Bayesian smoothing algorithm of the Viper software to find a plateau stability zone in the space (KN–α). Within the series of similar specimens, the values of (KN–α) optimized for one spectrum were usually suitable for the other spectra as well.

To obtain the true values of the strongly correlated Debye–Waller (σ^2) and coordination number (CN) parameters, decorrelation was carried out using multiple fits at different k-weightings. The series of fits at k-weightings from 1 to 3 were performed independently. Each time the σ^2 parameters for both sulfur and metallic second neighbor were fixed at some physically realistic values (in the range 0.002–0.015 Å ^{2}). Then a fit was run, and the CNs were determined. The resulting curves of the CN–σ^2 correlation obtained at different integer k-weighting values had an intersection point corresponding to the decorrelated value, as shown in Fig. 13 for the Co K edge of the Co-D specimen. At the intersection point, the quality of the fit passed through a maximum and became virtually equal for the different k-weighting values. Of course, even after this procedure some systematic errors in the CN determination are still possible, from other known and unknown sources, but comparison of the results within the same series of measurements becomes more reliable.

3.4.1. Cobalt K edge

Cobalt (nickel) K-edge spectra were measured for several reference compounds, including the precursors, the dried pre-catalysts, and the sulfided solids obtained from the TDM precursor. Because the TMM-derived solids contain large amounts

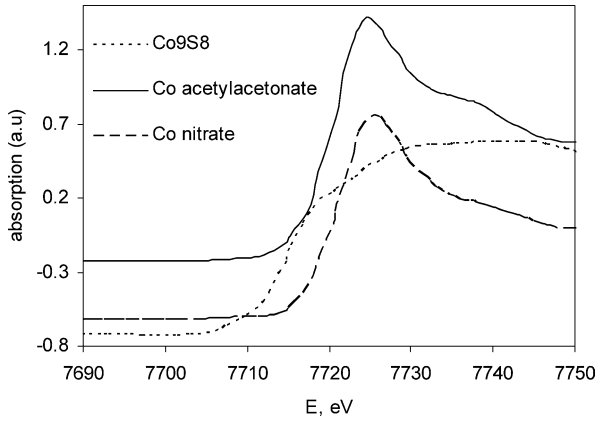

Fig. 14. Pre-edge and near Co K-edge regions for the spectra of the $Co(NO_3)_2 \cdot 6H_2O$ (a), $Co(acac)_2$ (b), and Co_9S_8 (c).

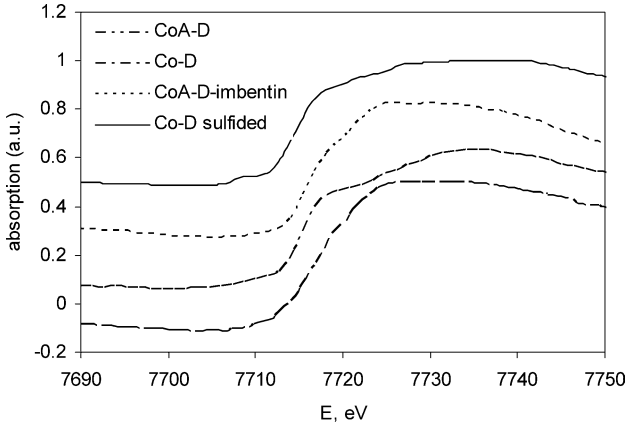

Fig. 15. Pre-edge and near Co K-edge regions for the spectra of several pre-catalysts and Co-D solid after sulfidation.

of XRD detectable Co_9S_8 after sulfidation, their EXAFS spectra were not measured. The pre-edge regions of the X-ray absorption spectra of Co nitrate, acetylacetonate, the Co_9S_8 reference, and our catalysts were analyzed using normalization of the edge jump, followed by subtraction of the background. The features at the pre-edge region can be related to the symmetry of the Co atoms, because the intensity of the pre-edge feature is greater for tetrahedral or distorted octahedral symmetry than for octahedral symmetry due to greater p–d mixing in the first case [57–59].

The Co K edges in the X-ray adsorption near-edge structures (XANES) region of the precursors, dry pre-catalyst, and sulfided solids are shown in Figs. 14 and 15. For all catalysts, the edge shape was changed from the precursor to the dry precipitate and then again on sulfidation. Analysis of the XANES of the precursor cobalt salts and the dried precipitates showed that the characteristic white line attributed to Co and Ni in the oxygen environment was absent in the pre-catalysts. A low intensity of the Co K-edge white line in the CoMoS pre-catalysts indicated an increased electron population in the cobalt (nickel) third level. At the same time, the energy position of the adsorption edges in the pre-catalysts shifted toward lower energies, in agreement with the sulfided state of the Co species [59–61]. A small but reliably determined pre-edge shoulder above

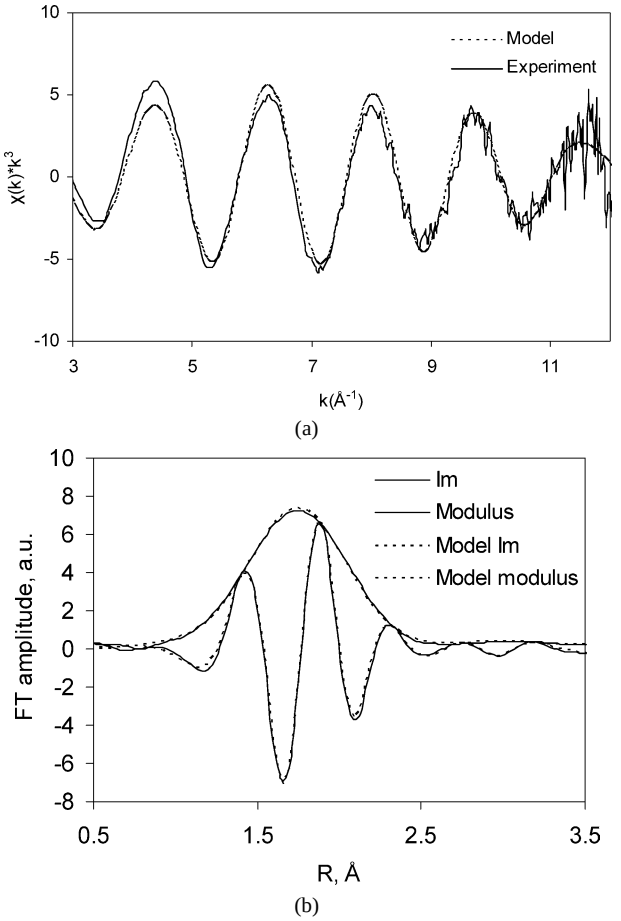

Fig. 16. Two-shell fit of the Co K-edge for the dried pre-catalyst Co-D in the k-space (a) and R space (b). Im—imaginary part.

7710 eV was observed in the spectra of the pre-catalysts, due to quadrupole and vibronically allowed 1s–3d transition (Fig. 15). Because a pre-edge peak is not expected for an octahedral coordination, this could be due to a tetrahedral or square-pyramidal environment of cobalt. This feature was absent in the cobalt nitrate and acetylacetonate precursors (Fig. 14). Thus we infer that the cobalt coordination changed from the oxygen octahedra in the precursors to the sulfur tetrahedra in the pre-catalysts. This conclusion was confirmed by the results of fitting the EXAFS spectra (Fig. 16). The quantitative analysis of the spectra (Table 3) showed that in the pre-catalysts, cobalt has about four sulfur neighbors and its coordination is tetrahedral rather than distorted octahedral. The fitting suggested the presence of molybdenum neighbors in the pre-catalysts. Treatment of the spectra using the difference file technique also confirmed the presence of this shell (Fig. 17a). The σ^2 parameter of closely bound sulfur was lower than that of the farther away molybdenum, presumably due to the high degree of static disorder in these solids.

After decomposition at 673 K, the local Co environment clearly changed. The k^3-weighted phase-corrected spectra showed the presence of a well-resolved feature at a distance of about 2.81 Å, probably corresponding to the Co–Mo contribution, similar to that of the "CoMoS phase" observed earlier [62,63]. Analysis of the phase-corrected spectra of the difference files confirmed this Co–Mo contribution (Fig. 17b). At the same time, the σ^2 parameter for the Co–S shell in the catalysts was systematically lower than that in the pre-catalysts, suggesting that some ordering occurred during the thermal activation. Formation of Co_9S_8 can be ruled out because in this case a strong Co–Co contribution should be seen at 2.50 Å due to the presence of most cobalt atoms in this structure within the Co_8 cubes [64]. Therefore, for all of the catalysts, the EXAFS spectra analysis, supported by the TEM results, suggests that the Co atoms were included mostly in the "Co–Mo–S" state (Table 3). The Co atoms in this state have a distorted five-fold sulfur coordination, and every Co atom is in contact with Mo atoms at a distance of 2.80–2.83 Å. As suggested in previous studies [62, 63], Co atoms are located in front of the square sulfur faces of the MoS_6 trigonal prisms along the edges of the MoS_2 crystallites. Note, however, that although the interatomic distances obtained in the fits correspond fairly well to previously reported data on the CoMoS phase, the coordination numbers obtained in this work were, for some unexplained reason, systematically lower than the values expected from the CoMoS phase model.

Table 3
Parameters resulting from the fit of Co(Ni) K-edge k^2-weighted EXAFS spectra for the unsupported catalysts and commercial references ($\Delta k = 3$–12 Å^{-1}, $\Delta R = 0.5$–4 Å)

Sample	Atom	R (Å)	δR	N	δN	σ^2 (Å^2)	ΔE (eV)	R (%)
Co-D–NH_3	S	2.21	0.0015	3.2	0.07	0.0093	2.2	4
	Co	3.14	0.004	1.1	0.1	0.0075	10.1	
Co-D	S	2.19	0.006	3.7	0.4	0.007	−1.6	12
	Mo	3.26	0.003	0.8	0.4	0.009	−5.0	
Ni-D	S	2.21	0.008	3.7	0.3	0.008	−1.4	16
	Mo	3.24	0.03	0.7	0.4	0.011	−5.2	
Ni-D sulfided ex situ	S	2.20	0.006	3.2	0.2	0.006	−2.1	11
	Mo	2.81	0.003	1.1	0.4	0.007	−4.3	
Ni-D Imbentin	S	2.19	0.007	3.6	0.5	0.009	−1.8	19
	Mo	3.25	0.03	0.8	0.4	0.013	−3.8	
Ni-D Imbentin sulfided ex situ	S	2.19	0.007	3.1	0.3	0.006	−2.4	14
	Mo	2.82	0.03	1.5	0.3	0.0065	−4.5	
NiA-D	S	2.20	0.008	3.4	0.4	0.009	−1.3	16
	Mo	3.27	0.03	0.6	0.4	0.012	−4.4	
CoA-D	S	2.19	0.008	3.5	0.4	0.009	−1.2	14
	Mo	3.24	0.04	0.7	0.4	0.012	−3.8	
CoA-D sulfided in situ	S	2.21	0.007	3.3	0.5	0.006	−2.0	15
	Mo	2.81	0.03	1.2	0.4	0.008	−4.5	
CoA-D sulfided ex situ	S	2.20	0.008	3.5	0.5	0.007	−1.5	14
	Mo	2.82	0.02	1.0	0.5	0.01	−5.0	
Co-D Triton X100	S	2.21	0.007	3.7	0.4	0.009	−2.0	18
	Mo	3.15	0.03	0.7	0.3	0.014	−6.1	
CoA-D Triton X114	S	2.21	0.008	3.8	0.3	0.0071	−1.2	11
	Mo	3.12	0.07	2.3	0.9	0.015	−4.6	
$CoMo/Al_2O_3$[a]	S	2.22	0.007	3.7	0.4	0.007	−0.5	14
	Mo	2.81	0.05	0.9	0.2	0.01	−3.2	

[a] Commercial reference.

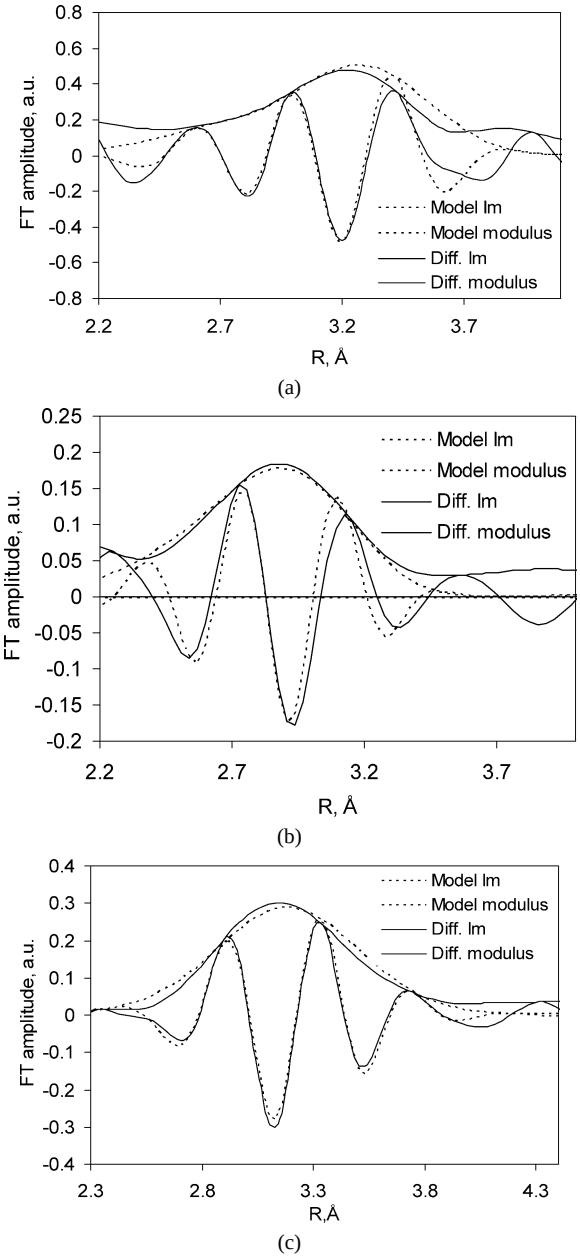

Fig. 17. Co K k^2-weighted EXAFS Fourier transforms of the difference $\chi(k)$ files (raw EXAFS minus Co–S contribution) for the second neighbours contributions: Co–Mo in the Co-D pre-catalyst (a), Co–Mo in the sulfided Co-D (b), and Co–Co in the Co-D-NH_3 (c). Solid curves correspond to the difference files; dashed curves represent the best fit model.

Further elucidation of the Co–Mo–S phase structure is beyond the scope of this work.

Considerable differences were also noted between pre-catalysts that provide highly active catalysts and those that do not. In the latter case, considerable Co–Co bonding was clearly observed both in the shape of the FT curves and in the difference files (Fig. 17c). Thus, for the amorphous Co-D–NH_3 pre-catalyst, a high-fidelity fit with decorrelation of CN and σ^2 provides evidence of the presence of a Co neighbor, suggesting the formation of the amorphous CoS compound. Replacing cobalt with molybdenum as a second neighbor significantly decreased the quality of the fit in the model, which no longer converged in k and R spaces. This excludes the formation of amorphous cobalt thiomolybdate for the Co-D–NH_3 solid. Apparently, at basic pH, reactions other than (1) and (2) occurred that included abstraction of sulfide ion from the TDM species and precipitation of cobalt sulfide, leading to a poor catalytic performance of this solid.

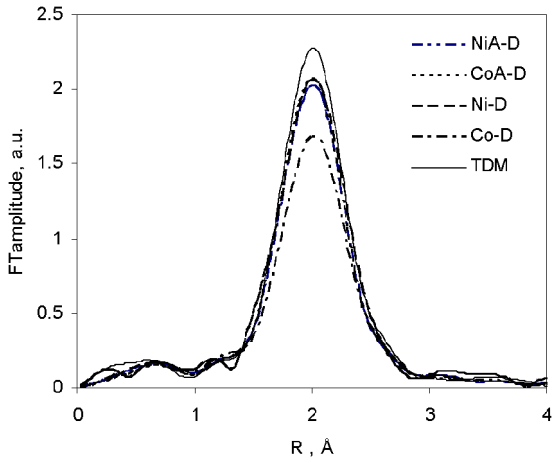

Fig. 18. FT module of Mo K EXAFS spectra of the ATDM precursor and several Co and Ni derived pre-catalysts.

3.4.2. Molybdenum K edge

Comparison of the absolute FT parts and k-weighted χ oscillations of the Mo K spectra revealed a remarkable similarity between the spectra of the TDM precursor and of several TDM-derived pre-catalysts (Fig. 18). Judging from the different backscattering amplitudes of the S and Mo atoms, the $\chi(k)$ oscillations corresponded mostly to the S shell. The second neighbor was not seen as a distinct peak or shoulder in the FT curves of the pre-catalysts and the imaginary part of the FT curves. However, analysis of the difference files and statistical analysis using the F test demanded introduction of the molybdenum shell.

The XANES of the TDM and pre-catalysts were nearly indistinguishable, indicating that the Mo_2S_{12} entities were preserved in the pre-catalysts. The TDM precursor has a complex structure in which the molybdenum atom has eight sulfur neighbors at distances ranging from 2.383 to 2.477 Å [65]. One molybdenum neighbor is present at 2.823 Å. Using the EXAFS spectrum of the TDM, we performed a fit with nine shells in which all distances and CN values were fixed and σ^2 and ΔE were varied but constrained to be equal for the same type of bonds (and thus this model has only four fitting parameters). Then the results for σ^2 and ΔE obtained for the TDM were taken as a departure point for a two-shell fit in which the distances and CNs were allowed to vary as free parameters (Fig. 19; Table 4). This simplification was necessary because it is impossible to obtain a reasonably converging fit using nine shells of the TDM structure. Apart from software performance limitations, the number of independent points in a typical measurement, $N_{\text{ind}} = 2\Delta k \Delta R/\pi$, is only about 25–30; however, to get an acceptable variance, the number of fit parameters should be considerably lower. But the CN values obtained for the ref-

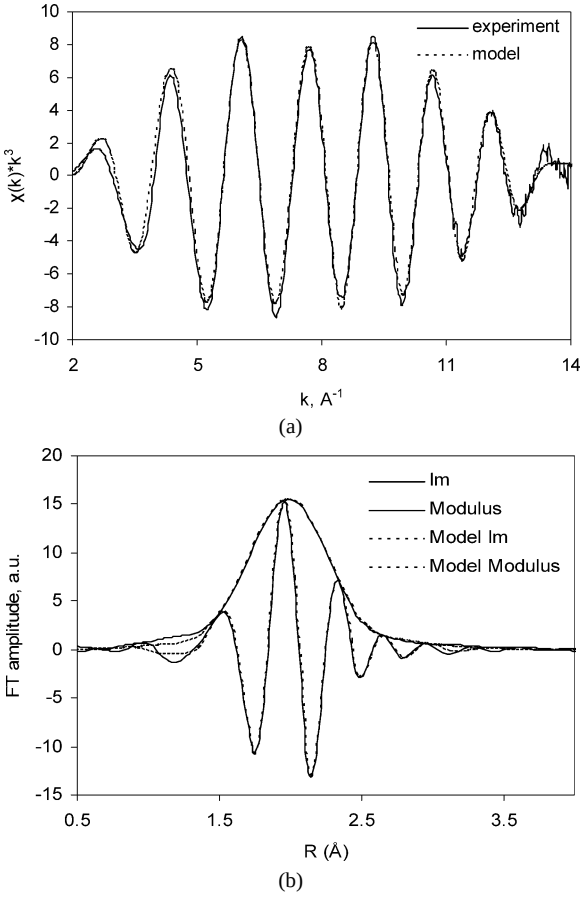

Fig. 19. Two-shell fit of Mo K edge in the Co-D dried pre-catalyst in the k-space (a) and R space (b).

Table 4
Parameters resulting from the fit of Mo K-edge k^2-weighted EXAFS spectra for the unsupported catalysts and commercial references (two shell model ($\Delta k = 2.5$–14 Å^{-1}, $\Delta R = 0.5$-4 Å))

Sample	Atom	R (Å)	δR	N	δN	$\Delta\sigma$ (Å^2)	ΔE (eV)	R (%)
TDM	S	2.440	0.005	5.8	0.2	0.0045	2.5	13
Precursor	Mo	2.823	0.01	1.0	0.15	0.0041	9.1	
Co-D–NH_3	S	2.450	0.009	5.8	0.5	0.0050	3.0	17
	Mo	2.815	0.02	1.2	0.8	0.0060	10	
Co-D	S	2.453	0.005	5.5	0.3	0.0063	3.4	9
	Mo	2.819	0.03	1.2	0.3	0.0061	8.75	
Co-D sulfided	S	2.40	0.007	4.6	0.5	0.0029	3.2	21
	Mo	3.17	0.02	3.0	0.8	0.0045	9.2	
Co-M	S	2.38	0.009	3.5	0.6	0.0080	2.3	19
	Mo	2.97	0.03	1.3	0.4	0.0110	9.0	
Ni-D	S	2.45	0.006	6.1	0.5	0.0055	1.7	9
	Mo	2.82	0.015	0.8	0.3	0.0050	7.8	
Ni-D sulfided	S	2.41	0.007	4.1	0.4	0.0029	1.6	20
	Mo	3.146	0.013	2.6	0.7	0.0042	8.0	
CoA-D Triton X114	S	2.448	0.007	5.7	0.4	0.0047	2.11	10
	Mo	2.834	0.028	1.0	0.2	0.0066	8.58	
Co-D Triton	S	2.451	0.007	6.1	0.4	0.0051	2.7	9
	Mo	2.818	0.02	0.9	0.15	0.0053	8.3	
Co-D Triton sulfided	S	2.408	0.007	4.7	0.5	0.0035	1.96	17
	Mo	3.168	0.015	2.9	0.9	0.0054	8.1	
CoA-D Triton X114	S	2.44	0.008	5.8	0.5	0.0056	2.5	14
	Mo	2.83	0.02	0.8	0.7	0.0065	9.0	

erence TDM specimen in the two-shell model fit were significantly lower than the real values. The reason for this apparent CN decrease was the spectral nonadditivity due to the phase differences between several scatterers having close but unequal distances. Indeed, a significant negative interference exists between sulfur scatterers in TDM positioned at 2.38 and 2.47 Å, as verified by direct comparison of the model spectra. Taking into account these limitations, the physical meaning of the fit parameters in this case should be considered a fingerprint of the averaged multiple Mo–S bonds. Analysis of Table 4 shows no important changes in the CNs and average distances of the precipitates compared with TDM. We found a slight increase of the average bond distance in the precipitates compared with the parent TDM and, as expected, higher σ^2 values for the Mo–S bonds in the disordered precipitates.

Earlier, Hibble and Feaviour applied a two-shell model in their study of the thermal decomposition of TDM [37]. The resulting molybdenum CN was significantly lower than it should be in the starting TDM material. To deal with this discrepancy, the authors had to introduce unrealistically high σ^2 factors (0.012 Å^2 in the crystalline TDM at room temperature). Using model clusters, Clausen et al. [66], Shido and Prins [67], and Calais et al. [68] demonstrated that CN is sensitive to the radial distribution of the bonds and is lower than its actual value when an asymmetric distribution is present and a normal data analysis is performed. Note that the asymmetric distribution of bonds is not equivalent to the effective increase in the static σ^2 parameter, because the spectrum damping at high k values is not the same in both cases. Obviously, stating a rigorous approach to the fitting problem is not possible at present.

Whatever the model applied to fit the spectra, it follows from our results that the Mo_2S_{12} moieties were preserved in the pre-catalysts. At the same time, the coordination sphere of cobalt was changed drastically. Therefore, we assume that the dithiomolybdate moieties were attached to cobalt with opening of the disulfide S–S bonds and formation of covalent Co–S bonds. The tentative structural sketch of the pre-catalyst is depicted in Fig. 20. In agreement with reaction (2), the chemical environment of molybdenum in the precipitates depended on neither the nature of the VIII group metal precursor nor the

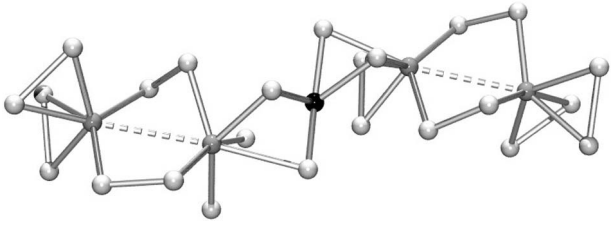

Fig. 20. Tentative model of the Co-D pre-catalyst structure. Light grey circles—S atoms; grey circles—Mo atoms; black circles—Co atoms. For better presentation not all the S atoms from the S–S groups are connected to the Mo atoms, even if they belong to the first coordination sphere.

nature of this last metal. Indeed, nearly perfect coincidence of the FT transforms was observed for the initial TDM and pre-catalysts obtained from the nitrate or acetylacetonate precursors. The same was true for the comparison of the nickel- and cobalt-containing pre-catalysts.

For the less important TMM-derived solids, we studied only one Co-M specimen at the Mo K edge. Obviously, the TMM- and TDM-derived solids exhibited large differences in the coordination shell parameters. A low coordination number suggests the presence of MoS_4 entities within the structure of the dried Co-M precipitate. Comparison of the spectra of Co-M and Co-D prepared under the same conditions showed considerably higher σ^2 values for the TMM-derived solid. A highly disordered amorphous $CoMoS_4$ compound can be envisaged as an adequate model to explain our observations.

Sulfidation led to the decrease in the sulfur CN and to the coordination shell ordering, related to a significantly decreased σ^2 parameter. In agreement with the formation of dispersed MoS_2, the molybdenum neighbors became more distant and increased in number. As is often observed in the EXAFS of dispersed MoS_2 catalysts, the coordination numbers obtained for both Mo and S were lower than the theoretical values. The presence of the cobalt neighbor could not be inferred from the Mo K-edge spectra of the Co–Mo–S systems, because the heavy and abundant molybdenum neighbor prevented the observation of a relatively small amount of cobalt.

Overall, the Co and Mo K-edge EXAFS of the pre-catalysts show that the thioanions preserved their chemical identity and the molybdenum coordination remained essentially the same as in the parent TDM. In contrast, cobalt changed its coordination from full oxygen coordination in the precursors to full sulfur coordination in the pre-catalysts, in agreement with reactions (1) and (2). A tetrahedral or a less common square-planar coordination of cobalt is compatible with our EXAFS data. The pre-catalysts was highly disordered, and the second metallic neighbor was difficult to see. After sulfidation, the solids were transformed to the dispersed CoMoS phase. Organics present in the solids did not noticeably influence the EXAFS spectra, and probably remained outside the chemical environment of the transition metals.

4. Conclusions

The study of unsupported or highly loaded supported sulfides is a promising research route for developing better hydrotreating catalysts. Solution preparations of macroporous and mesoporous transition-metal sulfides are particularly interesting, because they provide a possibility for tailor-made preparations. By controlling precursors, solvents, and reaction conditions, Ni(Co)–Mo–S catalytic materials can be prepared by structural and morphological tuning over microscopic- and mesoscopic-length scales. The preparations used in this work include room temperature surfactant-aided precipitations in mixed solvents. The reactions of the MoS_4^{2-} and $Mo_2S_{12}^{2-}$ cores with nickel or cobalt salts in mixed solutions produced amorphous solids (pre-catalysts) with a Ni(Co)/Mo ratio depending on the conditions and particularly on the nature of the thiomolybdate anion applied. Residual carbon in these solids played an important role in stabilizing their morphology and catalytic activity. Optimization of the promoted unsupported NiMo and CoMo systems allows us to obtain catalysts with very high activity in the HDS of thiophene and 4,6-DMDBT. The EXAFS study at the Co, Ni, and Mo edges clarified the coordination of the transition metals in the amorphous pre-catalysts and Ni(Co)MoS sulfided phases.

Many future improvements in these systems can be envisaged. Although their specific activity is very high, their intrinsic performance is still lower than that of supported catalysts, because many Mo atoms remain inaccessible for catalytic reactions. Thus, further improvement of the molybdenum dispersion remains possible. Thiomolybdates and ammonium sulfide are not really basic chemicals; furthermore, the amounts of organic compounds in the solutions are relatively high, making large-scale preparations potentially expensive. Therefore, the solution reaction should be simplified to obtain mixed sulfides in one step. The next challenge will be to prepare these in aqueous solution using simple precursors, such as ammonium molybdate or molybdic acid, commercially available cobalt salts, and cheap and nontoxic sulfur sources, the best one being elemental sulfur.

References

[1] C. Song, Catal. Today 86 (2003) 211.
[2] C. Song, X. Ma, Appl. Catal. B 41 (2003) 207.
[3] I.V. Babich, J.A. Moulijn, Fuel 82 (2003) 617.
[4] S. Brunet, D. Mey, G. Pérot, C. Bouchy, F. Diehl, Appl. Catal. A 278 (2005) 143.
[5] S. Mayo, E. Brevoord, L. Gerritsen, F. Plantenga, Hydrocarbon Process. 2 (2001) 84A.
[6] C. Olsen, L.D. Krenzke, B. Watkins, in: Proceedings of the Fifth International Conference on Refinery Processing, AIChE 2002 Spring National Meeting, New Orleans, LA, 11–14 March, 2002, p. 305.
[7] R. Candia, O. Sørensen, J. Villadsen, N.-Y. Topsøe, B.S. Clausen, H. Topsøe, Bull. Soc. Chim. Belg. 93 (1984) 763.
[8] J.A.R. van Veen, E. Gerkema, A.M. van der Kraan, A. Knoester, J. Chem. Soc., Chem. Commun. 22 (1987) 1684.
[9] J.A.R. van Veen, H.A. Colijn, P.A.J.M. Hendriks, A.J. van Welsenes, Fuel Proc. Technol. 35 (1993) 137.
[10] S.M.A.M. Bouwens, M.P. van Dijk, A.M. van der Kraan, D.C. Koningsberger, F.B.M. van Zon, V.H.J. de Beer, J.A.R. van Veen, J. Catal. 146 (1994) 375.
[11] H. Topsöe, B.S. Clausen, Catal. Rev.-Sci. Eng. 26 (1984) 395.
[12] R.R. Chianelli, M. Daage, M.J. Ledoux, Adv. Catal. 40 (1994) 177.
[13] R.R. Chianelli, M. Daage, J. Catal. 149 (1994) 414.
[14] G. Alonso, V. Petranovskii, M. Del Valle, J. Cruz-Reyes, A. Licea-Claverie, S. Fuentes, Appl. Catal. A 197 (2000) 87.
[15] G. Alonso, M. Del Valle, J. Cruz-Reyes, A. Licea-Claverie, V. Petranovskii, S. Fuentes, Catal. Lett. 52 (1998) 55.
[16] G. Berhault, L. Cota, A. Duarte, A. Mehta, R.R. Chianelli, Catal. Lett. 78 (2002) 81.
[17] Y.Y. Peng, Z.Y. Meng, C. Zhong, J. Lu, W.C. Yu, Z.P. Yang, Y.T. Qian, J. Solid State Chem. 159 (2001) 170.
[18] Y.Y. Peng, Z.Y. Meng, C. Zhong, J. Lu, W.C. Yu, Y.B. Jia, Y.T. Qian, Chem. Lett. (2001) 772.
[19] W.J. Li, E.W. Shi, J.M. Ko, Z.Z. Chen, H. Ogino, T. Fukuda, J. Cryst. Growth 250 (2003) 418.
[20] E. Devers, P. Afanasiev, B. Jouguet, M. Vrinat, Catal. Lett. 82 (2002) 13.
[21] N. Rueda, R. Bacaud, M. Vrinat, J. Catal. 169 (1997) 404.
[22] P. Afanasiev, G.F. Xia, G. Berhault, B. Jouguet, M. Lacroix, Chem. Mater. 11 (1999) 3216.

[23] I. Bezverkhyy, P. Afanasiev, M. Lacroix, Inorg. Chem. 39 (2000) 5416.
[24] I. Bezverkhyy, P. Afanasiev, C. Geantet, M. Lacroix, J. Catal. 204 (2001) 495.
[25] I. Bezverkhyy, P. Afanasiev, M. Lacroix, J. Catal. 230 (2005) 133.
[26] Y. Ji, P. Afanasiev, M. Vrinat, W. Li, C. Li, Appl. Catal. A 257 (2004) 157.
[27] C. Coyle Lee, T.R. Halbert, W.H. Pan, M.A. Harmer, L. Wei, M.E. Leonowicz, C.O.B. Dim, K.F. Miller, A.E. Bruce, S. McKenna, J.L. Corbin, S. Wherland, E.I. Stiefel, Inorg. Chim. Acta 243 (1996) 147.
[28] J.J. Rehr, S.I. Zabinsky, R.C. Albers, Phys. Rev. Lett. 69 (1992) 3397.
[29] K.V. Klementiev, J. Phys. D: Appl. Phys. 34 (2001) 209.
[30] J.B.A.D. van Zon, D.C. Koningsberger, H.F.J. van't Blik, D.E. Sayers, J. Chem. Phys. 82 (1985) 5742.
[31] R. Candia, B.J. Clausen, H. Topsøe, Bull. Soc. Chim. Belg. 90 (1981) 1225.
[32] J. Cruz-Reyes, M. Avalos-Borja, M.H. Farías, S. Fuentes, J. Catal. 137 (1992) 232.
[33] P. Afanasiev, I. Bezverkhyy, Chem. Mater. 14 (2002) 2826.
[34] R.R. Chianelli, G. Berhault, Catal. Today 53 (1999) 357.
[35] J.L. Brito, M. Ilija, P. Hernández, Thermochim. Acta 256 (1995) 325.
[36] A. Leist, S. Stauf, S. Löken, E.W. Finckh, S. Lüdtke, K.K. Unger, W. Assenmacher, W. Mader, W. Tremel, J. Mater. Chem. 8 (1998) 241.
[37] S.J. Hibble, M.R. Feaviour, J. Mater. Chem. 11 (2001) 2607.
[38] W. Eltzner, M. Breysse, M. Lacroix, M. Vrinat, Polyhedron 5 (1986) 203.
[39] A. Müller, E. Diemann, A. Branding, F.W. Baumann, M. Breysse, M. Vrinat, Appl. Catal. 62 (1990) L13.
[40] M. Draganjac, E. Simhon, L.T. Chan, M. Kanatzidis, N.C. Baenziger, D. Coucouvanis, Inorg. Chem. 21 (1982) 3321.
[41] W.H. Pan, M.A. Harmer, T.R. Halbert, E.I. Stiefel, J. Am. Chem. Soc. 106 (1984) 459.
[42] A.I. Hadjikyriacou, D. Coucouvanis, Inorg. Chem. 26 (1987) 2400.
[43] C. Glasson, C. Geantet, M. Lacroix, F. Labruyere, P. Dufresne, J. Catal. 212 (2002) 76.
[44] D. Nicosia, R. Prins, J. Catal. 229 (2005) 424.
[45] D. Nicosia, R. Prins, J. Catal. 231 (2005) 259.
[46] B.C. Gates, H. Topsøe, Polyhedron 16 (1997) 3213.
[47] T. Koltai, M. Macaud, A. Guevara, E. Schulz, M. Lemaire, R. Bacaud, M. Vrinat, Appl. Catal. A 231 (2002) 253.
[48] V. Meille, E. Schulz, M. Lemaire, M. Vrinat, J. Catal. 170 (1997) 29.
[49] E. Lecrenay, K. Sakanishi, I. Mochida, Catal. Today 39 (1997) 13.
[50] T. Isoda, S. Nagao, X. Ma, Y. Korai, I. Mochida, Appl. Catal. A 150 (1997) 1.
[51] T. Chiranjeevi, G. Muthu Kumaran, J.K. Gupta, G. Murali Dhar, Catal. Commun. 6 (2005) 101.
[52] M. Sun, D. Nicosia, R. Prins, Catal. Today 86 (2003) 173.
[53] Usman, T. Kubota, Y. Araki, K. Ishida, Y. Okamoto, J. Catal. 227 (2004) 523.
[54] M. Daage, R.R. Chianelli, J. Catal. 149 (1994) 414.
[55] V. Petkov, J. Appl. Crystallogr. 22 (1989) 387.
[56] C.H. Chang, S.S. Chan, J. Catal. 72 (1981) 139.
[57] J.M. Ramallo-Lopez, E.J. Lede, F.G. Requejo, J.A. Rodriguez, J.Y. Kim, R. Rosas-Salas, J.M. Dominguez, J. Phys. Chem. B 108 (2004) 20005.
[58] F.M.F. de Groot, J. Electron Spectrosc. Relat. Phenom. 67 (1994) 529.
[59] P.W. de Bont, M.J. Vissenberg, V.H.J. de Beer, J.A.R. van Veen, R.A. van Santen, A.M. van der Kraan, J. Phys. Chem. B 102 (1998) 5876.
[60] O. Kleifeld, L. Rulısek, O. Bogin, A. Frenkeļ, Z. Havlas, Y. Burstein, I. Sagi, Biochemistry 43 (2004) 7151.
[61] O. Proux, J.S. Micha, J.R. Regnard, A. Traverse, B. Dieny, F. Ernult, P. Bayle-Guillemaud, J.L. Hazemann, L. Giacomoni, J. Phys. Condens. Matter 15 (2003) 7237.
[62] S.M.A.M. Bouwens, J.A.R. van Veen, D.C. Koningsberger, V.H.J. de Beer, R. Prins, J. Phys. Chem. 95 (1991) 123.
[63] R.G. Leliveld, J.A.J. van Dillen, J.W. Geus, D.C. Koningsberger, M. de Boer, J. Phys. Chem. B 101 (1997) 11160.
[64] V. Rajamani, C.T. Prewitt, Can. Miner. 13 (1975) 75.
[65] A. Mueller, S. Pohl, M. Dartmann, J.P. Cohen, M.J. Bennett, R.M. Kirchner, Inorg. Chim. Acta 41 (1980) 259.
[66] B.S. Clausen, H. Topsøe, L.B. Hansen, P. Stoltze, J.K. Nørskov, Catal. Today 21 (1994) 49.
[67] T. Shido, R. Prins, J. Phys. Chem. B 102 (1998) 8426.
[68] C. Calais, N. Matsubayashi, C. Geantet, Y. Yoshimura, H. Shimada, A. Nishijima, M. Lacroix, M. Breysse, J. Catal. 174 (1998) 130.